Supporting Information

Supporting Tables

Table S1. Saturation and reproducibility of VCA-Arp2/3 stoichiometry.

[VCA*] (μM)	$[VCA^*]_{fast}$ (μM)	[Arp2/3] (μM)	VCA^*_{fast}/Arp2/3 Ratio	Comment
9.86	1.07	0.55	1.94	Optimized conditions†
9.86	1.11	0.54	2.03	Optimized conditions†*
14.4	0.69	0.38	1.82	$OD_{496} > 1$
14.3	1.4	0.79	1.77	$OD_{496} > 1$
4.71	1.52	0.87	1.75	Using OD_{312}
6.44	1.62	0.87	1.86	Using OD_{312}
10.3	1.83	0.86	2.13	Using OD_{312}
13.3	1.98	0.90	2.20	Using OD_{312}

† Conditions chosen to balance an $OD_{496} \sim 0.8$ (at the 12 mm pathlength) and the fast sedimenting VCA* species > 0.08 OD_{496}.

* Experiment shown in Fig. 1A. Data are also presented in reference (24).

Table S2. Summary of published data considered during construction of VCA binding site model.

Table S2. Part 1, Conformation of Arp2/3 Complex

Structure Observed	Method	Comment	Reference
Inhibited conformation of Arp2/3 complex	X-ray Crystallography	Forms the basis for all Arp2/3 structural modeling	(1)
Model of Arp2 in complex	Homology	actin-Arp2 similarity used to make a more complete model of the inhibited Arp2/3 complex structure	(2)
Arp2 and Arp3 reorient when bound to GST-CA	FRET	CA binding induces a conformational change	(3)
Arp2 and ArpC5 move upon VCA binding	EM	Negative stain, 3D reconstruction of complex of VCA and Arp2/3 complex shows rearrangement	(4)
Multiple Arp2 conformations	EM	Negative stain, projections and 3D reconstructions	(5)
VCA:actin bound to Arp2/3 complex	SAXS	Arp2 in short pitch contact with Arp3, first actin delivered to Arp2	(6)
Structure of Arp2/3 complex in the filament branch	Cryo-EM	Arp2 and Arp3 in short pitch contact, ArpC1 and ArpC3 have minor movements	(7)

Table S2. Part 2, Subunits of Arp2/3 Complex Bound by VCA

Contact Identified	Method	Comment	Reference
WAVE1 VCA contacts Arp3, Arp2 and ArpC1	Crosslinking	EDC-NHS/Western method	(8)
WAVE1 VCA contacts ArpC3	Crosslinking	EDC-NHS/Western method	(9)
N-WASP VCA contacts ArpC5	Crosslinking	EDC-NHS/Western method	(9)
GST-N-WASP VCA contacts Arp3, Arp2 and ArpC1 (and possibly ArpC3)	Crosslinking	EDC-NHS method, detected by Western	(10)
Cortactin NtA contacts Arp3 (and possibly Arp2, ArpC2 and ArpC3)	Crosslinking	EDC-NHS method, detected by Western	(10)
NtA competes for VCA binding to Arp3 but not for VCA binding to ArpC1	Crosslinking	EDC-NHS method, detected by western.	(10)
Conserved surfaces on Arp2, Arp3 and ArpC1	Homology	Identify several conserved surfaces, we use A-1, A-2, C-2 and M-3 here	(2)
N-WASP CA contacts Arp3, Arp2, ArpC1 and ArpC3	Crosslinking	Photoactivated ruthenium(II) crosslinking	(11)
N-WASP CA and Cortactin NtA can bind Arp2/3 complex simultaneously	FRET	Arp2/3 dependent FRET signal	(12)

Table S2. Part 3, Site Specific Information Within VCA

Contact Identified	Method	Comment	Reference
Truncation of acidic region affects crosslinking pattern	Crosslinking	EDC-NHS/Western Result of acidic deletion: Arp3 > ArpC1 >> Arp2	(10)
C- and acidic regions bind Arp2/3	NMR line broadening	C-region proposed to bind Arp2/3 through amphipathic helix	(13)
VCA:ArpC1	Direct binding	dependent on W503, suggesting acidic region contacts ArpC1	(14)
V region similar to C region	Homology	Proposes that C region binds Arp2 in fashion similar to V region binding actin	(6, 15, 16)
V-region:actin structure	X-ray crystallography	High resolution structure of VCA bound to actin	(17)
Arp3:N-WASP CA A462DOPA	Crosslinking	Oxidation induced crosslinking with synthetic peptide with A462DOPA	(11)
A462C > 25 Å from ArpC3 A481C < 25 Å from ArpC3 C506 < 25 Å from ArpC3	NMR line broadening	Isotope labeled ArpC3 methyl group NMR signals examined for broadening by nitroxide spin label	(11)
C-region:ArpC1	Crosslinking	EDC:NHS crosslinking, C-region is isolated peptide	(18)
CA contacts to Arp2, Arp3, ArpC1 and ArpC3	Crosslinking	Resolved to donor site on CA, also competition with NtA	Figure 3 and S3, this study

Table S2. Explanation of Method Classes.

Crosslinking: Methods that generates covalent crosslinks between CA or VCA and Arp2/3 subunits.

Direct binding: Demonstration of an interaction of VCA with a purified Arp2/3 subunit (only for ArpC1).

EM/Cryo-EM: Electron microscopy, negative stained or frozen hydrated samples, respectively.

NMR line broadening: Use of nuclear magnetic resonance signals, and their broadening by an introduced spin label or by association with the slowly tumbling Arp2/3 complex.

SAXS: Small angle X-ray scattering.

X-ray crystallography: High-resolution structural model determined using x-ray diffraction of protein crystals.

Y2H: Contact determined using the yeast two hybrid method.

Supporting Figures

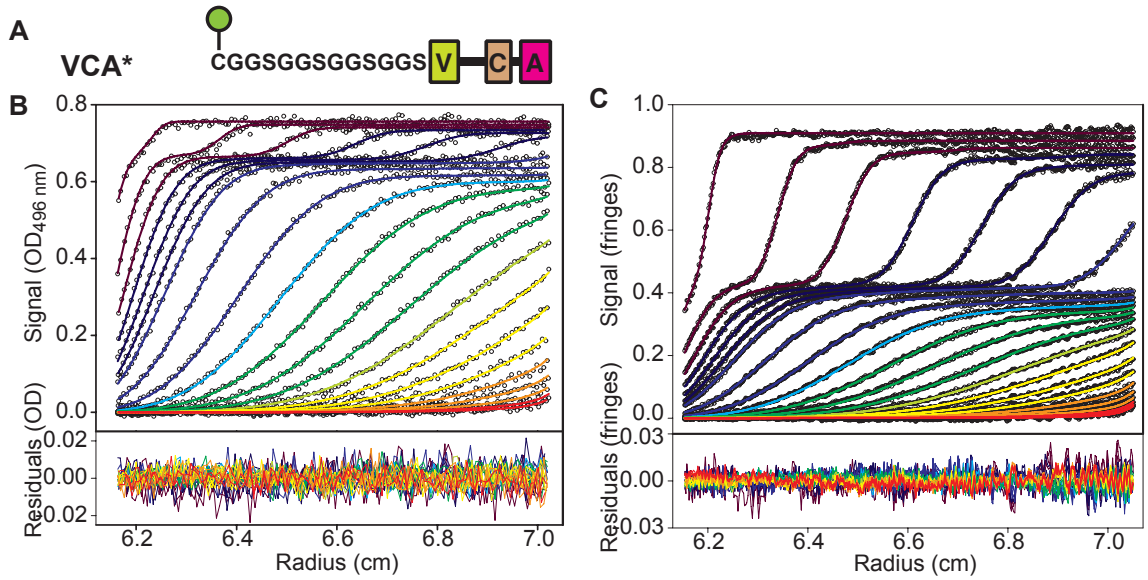

Figure S1. Multisignal Sedimentation Velocity Data

Sedimentation velocity analytical ultracentrifugation experiments of 0.54 μM Arp2/3 complex and 9.9 μM VCA* in AUC buffer, were collected using absorbance at 496 nm and interference signals. (A) A cartoon indicating the labeling of N-terminal C(GGS)4 linker on human WASP VCA. The AlexaFluor488-maleimide dye label is indicated by a green circle. (B) and (C) Data shown is every third data point for every third scan used in the analysis. Smooth lines are results of a multisignal global fit of the sedimentation velocity data performed in SEDPHAT. Fits to early times are in purple, intermediate times in green and late times in red. Data in panels B and C are also appear in reference (24).

A

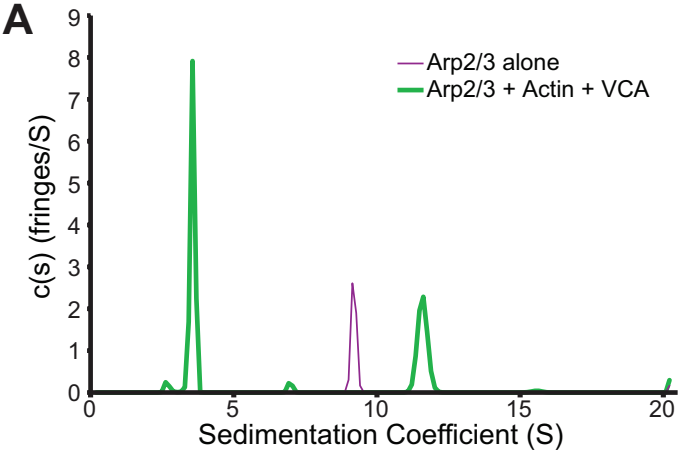

B

Proteins in Experiment	Sedimentation Coefficient (S)	Fringes in peak	Measured Mass (kDa)	Predicted Mass (kDa)
Actin	3.5	1.65	46.9 (46.3 - 47.5)	42
VCA	-	-	not done	-
Arp2/3	9.2	0.66	218 (217 - 220)	224
Actin + Arp2/3	9.2	0.66	238 (230 - 246)	224 (for Arp2/3 alone)
VCA + Actin	3.4	2.0	51.9 (51.6 - 52.3)	50
VCA + Arp2/3	9.6	0.73	237 (233-241)	241 (for 2:1 complex)
VCA + Actin + Arp2/3	11.4	0.98	333 (327 - 340)	324 (for 2:2:1 complex)

Figure S2. Stoichiometry determined from molecular weight estimates

Sedimentation velocity analytical ultracentrifugation experiments with 0.9 μM Arp2/3 complex, 12 μM N-WASP VCA (second V-region only) and 12 μM actin. Latrunculin B was added to prevent actin polymerization. (A) *c*(*s*) distributions were derived for Arp2/3 alone (thin purple line), or for a mixture of Arp2/3, VCA and actin (thick green line). Peaks with the indicated sedimentation coefficient were used to calculate masses. (B) Sedimentation coefficients, fringes of signal in the peak, measured and predicted masses are reported for interference detected sedimentation time courses. Concentrations for Arp2/3, VCA and actin (when present) are 0.9 μM, 12 μM and 12 μM, respectively. Numbers in parenthesis following mass estimate are the 1σ confidence interval for fitting

of the mass value. For each experiment, only the peak with the largest sedimentation coefficient is reported. Data were collected at 30,000 rpm.

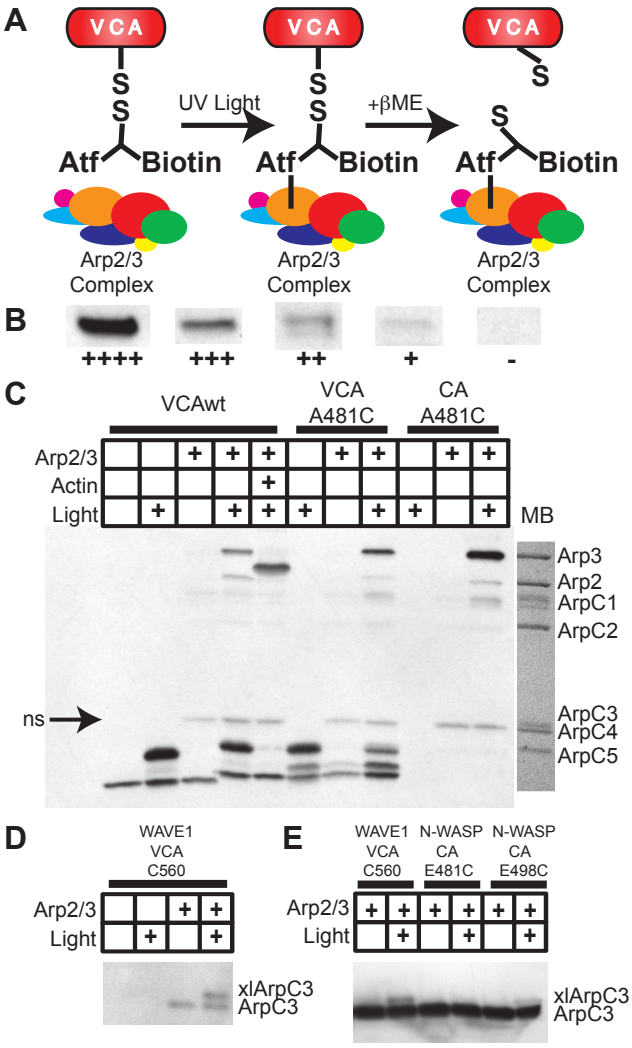

Figure S3. Label transfer and crosslinking controls

(A) Cartoon representation of the label transfer method employed here. Cartoon representation of the Mts-Atf-Biotin crosslinker (Pierce) following coupling to VCA. "Atf" indicates the 4-azido-2,3,5,6-tetrafluorobenzoyl photoactivatable crosslinker. βME is beta-mercaptoethanol, which is used to reduce the disulfide bond. The spacer arm between the disulfide bond and the Atf can span ~11 Å (see manufacturer instructions),

but the Atf itself has ~6 Å between the spacer arm and the reactive azido group, for a total range of ~17 Å. (B) Band intensities were scored empirically, reference intensities are given. ArpC2 typically showed some anti-biotin staining in the absence of illumination, thus it was scored as negative unless the staining increased appreciably (true for NtA-Cys). ArpC3 also showed some cross reaction, but label transfer could be identified by altered mobility (see below). (C) Arp2/3 and N-WASP VCA or CA label transfer donors were mixed and, where indicated, illuminated. Wild type N-WASP VCA contains a cysteine (C431) between its two V regions, which is mutated to alanine in all other VCA donors, and is missing in the CA donors. Biotinylated Arp2/3 subunits were visualized using Neutravidin-HRP and identified by comparison to the Memcode Blue stained blot (Labeled MB). Nonspecific cross-reaction with ArpC3 is indicated with "ns". Label transfer to ArpC3 results in a mobility shift. (D) Neutravidin-HRP blot for biotin following label transfer to Arp2/3 complex from WAVE1 VCA C560 Atf-Biotin donor. Sample composition and illumination are as indicated. The band marked ArpC3 results from nonspecific cross reaction of Neutravidin-HRP with ArpC3 observed in all blots. The additional band in the illuminated, Arp2/3 containing sample, labeled "xlArpC3", is a label transfer product. This band is also observed for N-WASP VCA C506 and N-WASP CA E498C donors. (E) Western blot with anti-ArpC3 antibody. All samples have Arp2/3 and the indicated VCA donor. Where indicated, samples were illuminated. WAVE1 VCA C560 donor samples are the same as those in panel. The intense band (labeled ArpC3) is unreacted ArpC3, additional band (labeled xlArpC3) in the illuminated lanes for WAVE1 VCA C560 and N-WASP CA E498C donors corresponds to the mobility seen for the additional band in (D).

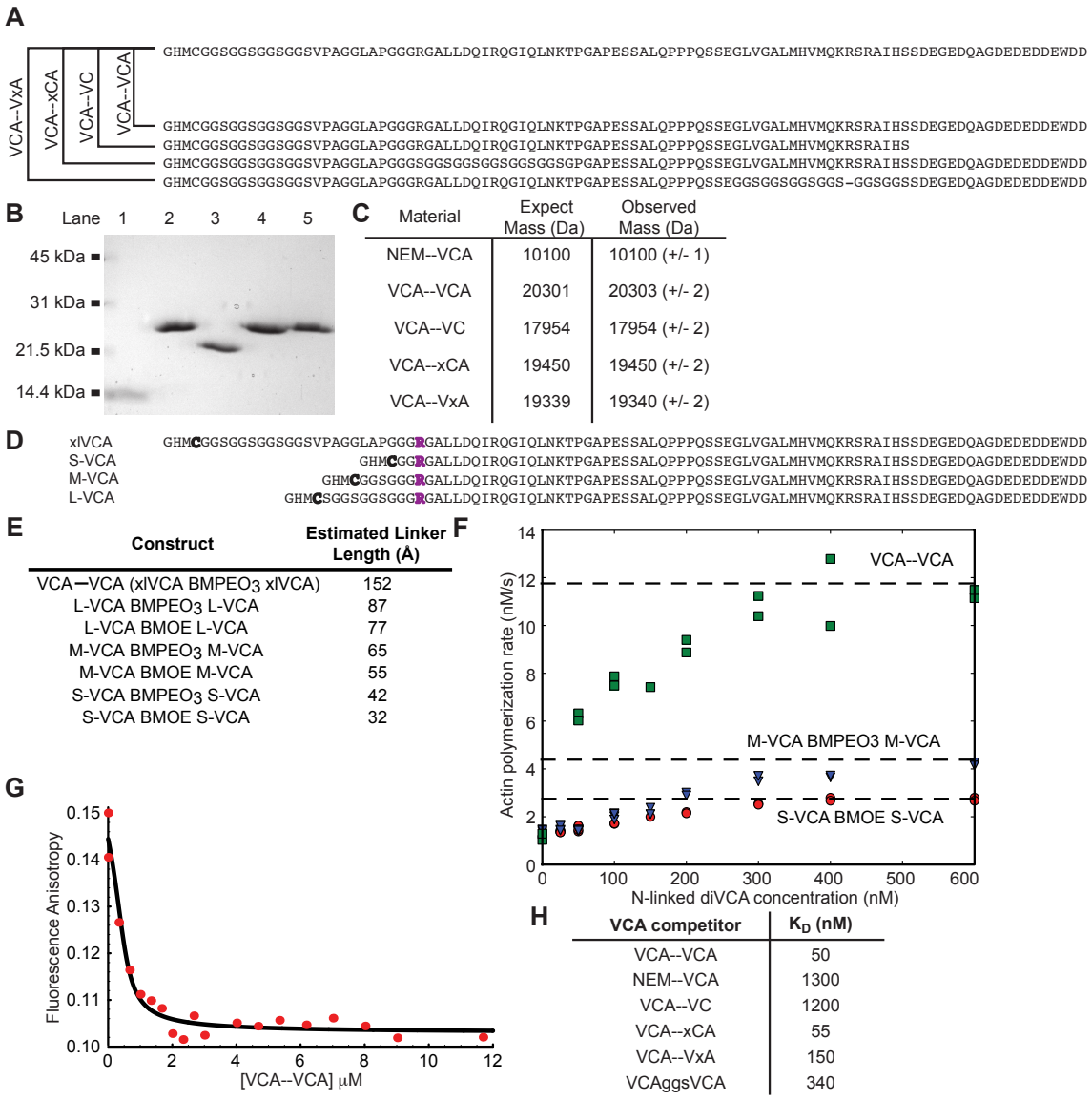

Figure S4. Modified VCA—VCA dimers

(A) Detail of truncations and GGS linker substitutions used in VCA—VCA materials. Vertical bar connecting the protein sequences indicates coupling via $BM(PEO)_3$ crosslinker. NEM—VCA is the top sequence coupled to N-ethyl maleimide. (B) SDS-PAGE of the final VCA—VCA heterodimers. Lane 1, NEM-VCA; lane 2, VCA—VCA;

Supporting Information

lane 3, VCA—VC; lane 4, VCA—xCA; lane 5, VCA—VxA. Molecular weight standards are indicated at left. (C) Final product identity was confirmed by ESI-MS. Table of expected and observed masses for the materials in (B). (D) Details of the WASP VCA variants used in the N-terminal linker experiment. xlVCA is the form of VCA used in the heterodimer experiments. The cysteine used to crosslink the VCAs together is indicated in black bold text. The first ordered residue in the WASP V:actin structure is indicated in bold purple (arginine). Different linkers are appended before this arginine. (E) The estimated N-terminal linker lengths for the VCA dimers. Linker length was estimated as Length = 2 x (2.8 Å per linker residue + 4 Å for the cysteine side chain coupling to maleimide) + crosslinker length. Crosslinker lengths are estimated as 8 Å for BMOE and 18 Å for $BMPEO_3$. The linker residues are counted from the arginine in bold purple in panel (D). (F) Activity in actin polymerization assay found for the N-linked VCA dimer constructs: S-VCA BMOE S-VCA (red circles), M-VCA BMPEO3 M-VCA (inverted blue trianlges) and VCA—VCA (green squares). Activity shown is the actin polymerization rate at t_{50} for individual reactions. The horizontal dashed line near each material name is an approximate saturating activity, determined by eye. (G) Representative fluorescence anisotropy data for VCA—VCA competition against 25 nM N-WASP VCA C506-Alexa488 maleimide reporter and 500 nM Arp2/3 complex. (H) Affinity of VCA materials for Arp2/3 complex measured in competition binding assay. All affinity measurements made in KMEI.

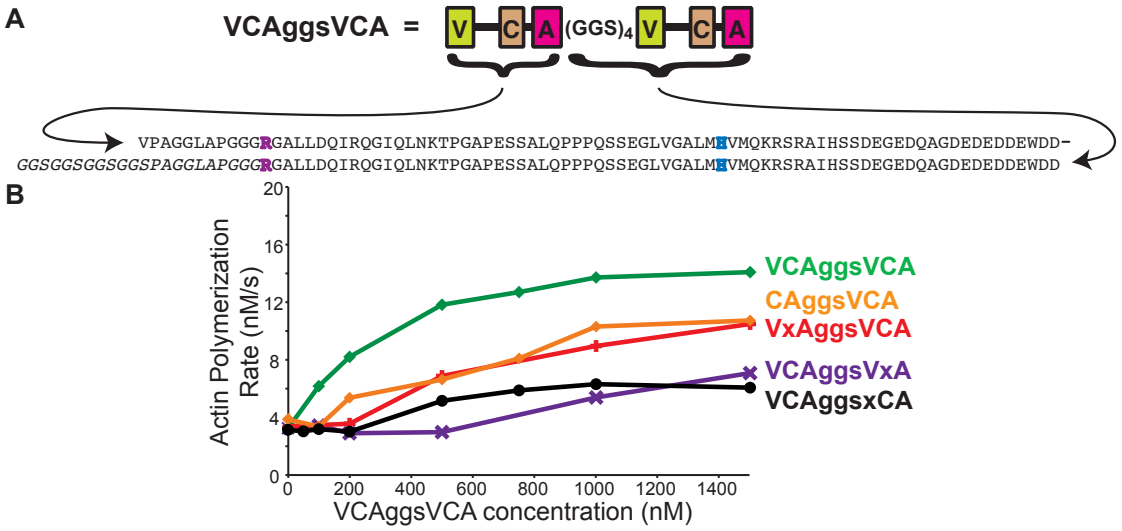

Figure S5. Activity of VxAggsVCA and VCAggsVxA

(A) The amino acid sequence of the VCAggsVCA material. The first ordered residue of the V-region is the arginine indicated in bold purple. Linker residues are in italic, there are 22 residues in the linker and it is estimated that they can span 61 Å. The dash at the end of the first line indicates that the first line and second line are connected sequence. The label transfer donor position used in Fig. 5B, H472, is indicated in bold blue. The sequence of VCAggsxCA, CAggsVCA, VxAggsVCA, and VCAggsVxA can be inferred from the relevant counterparts in Figure S4A.

(B) Actin polymerization rates in Arp2/3 dependent actin polymerization assays stimulated with the indicated concentrations of VCAggsVCA derived materials, 10 nM Arp2/3, and 4 μM actin (5% pyrene labeled) in KMEI150. Data for VCAggsVCA, CAggsVCA and VCAggsxCA are the same as that in Figure 5. Data shown are single reaction analyses.

Supporting Information

Figures 4B and S5B show that deletion of one C-helix from the N-terminally linked dimer reduces the affinity for Arp2/3 complex, but does not negatively affect activity at saturation. However, mutation of the C-region in monomeric VCA substantially decreases saturating activity (13, 18). To explain this apparent disparity, we note that mutation of VCA monomer affects both sites on Arp2/3 complex, and propose that only one site is required for activity. Thus, the relatively high saturating activity of VCA—VxA could result from preferential binding of the VCA dimer in one of the two orientations, which activates Arp2/3 complex. This would be analogous to the argument regarding the V-region, except that the preferred orientation is the active one. In essence, if there are two binding sites for VCA on Arp2/3, and at one site, the C-region contributes more binding energy to the association, then deletion of one C-region will result in biasing of the remaining C-region to the site which yields a higher affinity. In the case of a single C-region deletion, this steers the C-region to the site where it also contributes more to the activation of Arp2/3. From the C-region deletions in the VCAggsVCA context shown here, we infer that the Arp3 directed C-region (mutated in VCAggsVxA) contributes more greatly to activation than the Arp2 directed C-region (mutated in VxAggsVCA).

Supplementary Materials and Methods

Cloning of expression constructs

N-WASP VCA (human N-WASP residues 393-505) and CA (human residues 458-505) were prepared using a previously described pGEX-2T derived vector. Expression construct for N-WASP single V region VCA (432-505) was produced from the N-WASP VCA construct and cloned into a Tev protease cleavable, pGEX-2T derived vector. Point mutations in N-WASP VCA and CA were made using QuickChange Site Directed mutagenesis (Stratagene). Vectors describing WASP VCA (human WASP residues 421-502) and Cortactin NtA (human cortactin residues 1-36) were described previously (12). WASP $c(ggs)_4$-VCA (where VCA is the human WASP VCA and $c(ggs)_4$ is the amino acid sequence CGGSGGSGGSGGS, appended to the VCA N-terminus) and Bt-*HRV3C*-$c(ggs)_4$-VCA (the c(ggs)4-VCA sequence with a basic tag (Bt), the amino acids KKRKRKRK, followed by the cleavage site for HRV 3C protease appended at the N-terminus) were prepared from the parent GST-fusion construct using conventional PCR and subcloning methods. The VCA derivatives $c(ggs)_4$-VC, $c(ggs)_4$-xCA and $c(ggs)_4$-VxA were prepared by PCR construction using appropriate primers. Codon-optimized WASP VCAggsVCA constructs (including mutants and deletions) were prepared by gene synthesis (IDT DNA, Coralville, Iowa, USA). The sequences of all expression constructs were verified by DNA sequencing.

Supporting Information

Protein Preparation

Actin, pyrene actin and Arp2/3 were prepared as previously described (19). Briefly, actin was prepared from rabbit muscle acetone powder, and labeled with pyrene iodoacetimide as described (20). Arp2/3 complex was purified from bovine thymus, following the method of Higgs et al. (21). All chromatography materials were from GE Healthcare.

Recombinant proteins were expressed in BL21(DE3) T1R cells grown in LB media (with 100 μg/ml ampicillin added) to an OD600 of ~0.8. Expression occurred at 37° C for 3-4 hours, and was induced by the addition of 1 mM IPTG. Exceptions include Cortactin NtA constructs, which were expressed at 20° C for 12 hours, and Bt-*HRV3C*-c$(ggs)_4$-VCA, which was expressed for 3-4 hours at 37° C in rich media using a ten liter bioreactor. Cells were lysed using a cell disruptor (Emulsiflex-C5, Avestin) and clarified by centrifugation.

N-WASP VCA, N-WASP single V-region VCA and N-WASP CA, WASP VCA and VCAggsVCA derived materials were produced as GST fusions, as described above. Following lysis and clarification as above, VCA materials were purified using DEAE Sepharose, Glutathione Sepharose 4B and cleaved using Tev protease overnight at 4°C. Following this, C-terminally truncated materials were removed using a gradient elution from SOURCE15Q column developed over 20 column volumes. Pooled fractions were frozen at this point until needed. Once thawed, materials were concentrated using a 500 μl SOURCE15Q column and applied to a Superdex200 column in KMEI (or AUC buffer, described below).

Supporting Information

Cortactin NtA was purified using glutathione sepharose followed by Tev protease cleavage. Following cleavage, NtA materials were further purified using SOURCE15Q and gel filtration (Superdex75) into KMEI. WAVE1 VCA materials for label transfer were purified using SP sepharose followed by MonoQ ion exchange chromatography, and then labeled as described below. WASP c$(ggs)_4$-VC was purified using glutathione sepharose followed by Tev protease cleavage and SOURCE15S cation exchange chromatography, and then coupled to c$(ggs)_4$-VCA as described below.

VCA—VCA, N-terminal linker variants, and N-terminally linked VCA heterodimers were purified differently depending on construct. Briefly, individual c$(ggs)_4$-VCA materials (c$(ggs)_4$-VCA, Bt-*HRV3C*-c$(ggs)_4$-VCA, c$(ggs)_4$-VxA, c$(ggs)_4$-xCA, short-VCA, medium-VCA and long-VCA) were purified through the MonoQ step described for WASP VCA (12). c$(ggs)_4$-VC was purified as described above. Materials were reduced with 2 mM DTT and quickly exchanged/concentrated in non-reducing buffer using a 500 μl SOURCE15Q ion exchange column (VC material using SOURCE15S instead). Materials were quantified using UV absorbance or relative gel staining and mixed at one to one ratios at individual concentrations of over 20 μM. Freshly prepared $BM(PEO)_3$ or BMOE (Pierce Biotechnology) in DMSO, was added at a ratio of 0.65 equivalents of the combined VCA concentration, separated into four aliquots and incubated for 15 minutes at room temperature between additions. Following crosslinking, VCA—VCA, N-terminal linker variants and VCA—VC were purified using SOURCE15Q and Superdex 75 chromatography into KMEI. Heterodimer materials with two acidic regions (VCA—xCA and VCA—VxA) could not be purified completely using the SOURCE15Q step

above, and were instead produced by crosslinking $c(ggs)_4$-xCA, or $c(ggs)_4$-VxA, to Bt-*HRV3C*-$c(ggs)_4$-VCA. The Bt (basic tag) greatly changes the interaction of the peptides with SOURCE15S resin and thus allowed the separation of the mixed crosslinking products by cation exchange chromatography. Following this step, the Bt tag was removed using cleavage by HRV 3C protease. Finally, anion exchange chromatography (SOURCE15Q) and gel filtration (Superdex75) into KMEI produced the final purified material.

Label transfer donor materials and WASP $c(ggs)_4$VCA (for production of VCA*) materials were purified through the MonoQ step as previously described for wild type materials then frozen (except WAVE1 VCA which was not frozen). Freshly thawed materials were reduced by the addition of buffered DTT, then exchanged into non-reducing conditions and concentrated using a 500 μL SOURCE15Q column. Eluted fractions were labeled with a ten-fold excess of dye (Alexa Fluor 488 C_5 maleimide, Invitrogen), to produce VCA*, or label transfer reagent (Profound Mts-ATF-Biotin, Pierce) for 2 hours at room temperature. Excess label transfer reagent was removed by gel filtration over Superdex75 into non-reducing KMEI. Excess dye was removed using ion exchange followed by gel filtration chromatography.

Following the final gel filtration column, all materials were used without further concentration or freezing. Concentration was determined using UV absorbance as 280 nm. The identity of the materials was verified by ESI-MS (QSTAR XL QTOF, Applied Biosystems), performed by the Protein Chemistry Technology Center at the University of Texas, Southwestern Medical Center.

Supporting Information

Analytical Ultracentrifugation

Experiments were carried out in an Optima XL-I centrifuge using an An50-Ti rotor (Beckman-Coulter, Indianapolis, IN). Except for actin, individual sample components were gel filtered into the same preparation of AUC buffer (5 mM HEPES pH 7.0, 50 mM KCl, 1 mM $MgCl_2$, 1 mM EGTA) and appropriate volumes were combined without concentration, diluting with additional AUC buffer. Actin was dialyzed into 2 mM Tris/HCl, 100 mM $CaCl_2$ and 200 μM ATP, pH 8.0, and latrunculin B was added from an ethanol stock. Samples (~390 μl) were placed in charcoal-filled, dual-sector Epon centerpieces and allowed to equilibrate at the experimental temperature (20° C) for several hours. Absorbance and/or interference optical systems were used to monitor the sedimentation of the proteins at a rotor speed of 50,000 rpm.

VCA-Arp2/3 stoichiometries were determined using mixtures of VCA* (WASP $c(ggs)_4$-VCA, coupled to AlexaFluor 488 maleimide Fig. S1A), Arp2/3 and NtA, at the indicated concentrations (Table S1 and Fig. 1). Concentrations were determined using the interference signal of the purified materials, and were calculated using an interference signal increment (which, in our analysis, was functionally equivalent to an extinction coefficient) of 2.75 times the molecular weight (22). Absorbance (at 496 nm or 312 nm as indicated) and interference data were acquired in parallel, see examples in Figure S1, panels B and C. The extinction coefficients of VCA* (ε_{496nm} = 65000 M^{-1} cm^{-1}, calculated from ε_{if} = 37186 M^{-1} cm^{-1} and absorbance at 496 nm of the free VCA* signal) and Arp2/3 complex (ε_{496nm} = 0 M^{-1} cm^{-1}, using ε_{if} = 615516 fringes M^{-1} cm^{-1}), were used to extract the concentrations of both components simultaneously throughout the experiment. This

allowed construction of $c_k(s)$ distributions for VCA* and Arp2/3 complex (see example in Fig. 1) using SEDPHAT (23), as described in (24). To reduce biasing of the analysis toward slow sedimenting species, we analyzed every scan for the first twenty scans, and every fourth scan thereafter (of roughly two hundred total scans).

In the $c_{VCA*}(s)$ distribution, the slowly sedimenting VCA* pool (~1.6 S) and the rapidly sedimenting (~9.3 S) pool, which cosediments with Arp2/3 complex, are well resolved (note the fast sedimenting portion of the signals in Fig. S1B and S1C; as indicated by the bi-sigmoidal sedimentation profile seen for most time points). By integrating the $c_k(s)$ peaks representing the fast sedimenting Arp2/3 and VCA* species (the shaded regions in Fig. 1A), we could determine the molar ratio of their complex. Under conditions of optimized absorbance at 496 nm, concentrations of 0.54 μM and 9.9 μM for Arp2/3 complex and VCA* respectively, we observed 1.1 μM of VCA* cosedimenting with Arp2/3 complex. This corresponds very closely to a 2:1 molar ratio. Based on the sedimentation coefficient of the complex, it was deduced that 2:1 is the proper stoichiometry of the interaction. The stoichiometries observed for eight separate experiments (Table S1), using different ratios of the components and multiple VCA* and Arp2/3 complex preparations, found most had a stoichiometry near two VCA*s per Arp2/3 complex, with the principal exception at the lowest VCA* concentration. As the 2:1 stoichiometry was found for a range of VCA concentrations, this likely represents a true saturating stoichiometry. For very high VCA* concentrations, absorbance at 312 nm was used instead of absorbance at 496 nm.

Supporting Information

For the titration of NtA into the VCA*:Arp2/3 mixture, [VCA*] and [Arp2/3] were held constant (9.9 μM and 0.54 μM, respectively), while the indicated concentrations of NtA (Fig. 1) were added to separate samples. The data were analyzed using a variant of described methods (23, 25, 26). In brief, the data were modeled with $c_k(s)$ distributions assuming that NtA makes a negligible contribution to the interference signal of Arp2/3 complex, which is reasonable given the relative masses of the two elements. See (24) for an extended discussion of this process.

To determine how many actin monomers can bind to the Arp2/3:VCA_2 dimer we made use of two related SVAUC methods. For both methods, only interference data were collected, which allowed acquisition of one scan of each sample per minute. The lack of salt in the actin stock was accounted for by using a 10x stock of AUC buffer, such that the final buffer conditions (for all samples in these experiments, when actin was not added, an equal volume of buffer G was added maintaining identical conditions) were 50 mM KCl, 5 mM HEPES pH7.0, 1 mM EGTA, 1 mM $MgCl_2$, 0.9 mM Tris pH8, 90 μM ATP, 0.45 mM Sodium Azide, 45 μM $CaCl_2$, 0.25% v/v ethanol, 50 μM Latrunculin B. AUC equipment was as described above. The freeware programs used for these analyses, SEDFIT and SEDPHAT, are available at http://www.analyticalultracentrifugation.com. The freeware program SEDNTERP (27) was used to estimate the values of buffer density, buffer viscosity, and partial specific volume. For these estimates, not all buffer components had tabulated information available in SEDNTERP. Therefore, EGTA was approximated as EDTA and Latrunculin B was ignored.

Supporting Information

The first measurement of actin association with the Arp2/3:VCA_2 assembly tracked the quantity of VCA-actin which changed from a slowly sedimenting pool to a rapidly sedimenting, Arp2/3 complex bound pool. For this methodology, a rotor speed of 50,000 rpm was used. This analysis determines the fraction of VCA:actin interference signal (in units of fringes) that cosediments with the rapidly sedimenting species, which contains Arp2/3 complex. Samples were prepared and acquired in parallel with particular care used to match component concentrations across samples. Input VCA, actin and Arp2/3 complex concentrations were determined by integration of the interference signal for the individual component samples, and using the signal increment calculation described above. For this experiment, VCA, actin and Arp2/3 complex concentrations were 11.5 μM, 11.2 μM and 1.04 μM, respectively. The VCA used in this case was the N-WASP VCA, but including only the sequence covering the second V-region through the C-terminal acidic region. VCA:actin simply refers to the complex of the two components. Total interference signal was separated into a rapidly sedimenting, "leading" portion of the interference signal ($s > 7$ *S*) and a slower sedimenting "lagging" portion of the interference signal ($s < 7$ *S*) (Fig. 2A and B) (25). Integrating the signal in each peak, in units of 'fringes' for this interference detected experiment, we can follow the loss or gain of mass as components are added (Fig. 2C). Tracking the "leading" peaks, 1.14 fringes of signal rapidly sediments in the Arp2/3, VCA, and actin mixture. The 1.04 μM Arp2/3 complex in the sample contributes 0.77 fringes (based on its ε_{if} value of 615,516 M^{-1} cm^{-1}, see (28)), leaving 0.37 fringes of leading signal from VCA:actin. This corresponds to 2.22 μM VCA:actin bound to Arp2/3 complex, for a ratio of ~2.1 VCA:actins per Arp2/3.

A very similar ratio is also found when the "lagging" VCA:actin peak is quantified (Fig. 2C). Thus, the two modes of accounting for the redistribution of VCA:actin agree with each other.

The second methodology was to use SVAUC to estimate the molecular weight of the VCA-actin-Arp2/3 complex assembly from hydrodynamic properties. For this methodology a rotor speed of 30,000 rpm was chosen, which emphasizes diffusion in the larger species. This speed was not fast enough to completely sediment N-WASP VCA. The masses were estimated using a hybrid discrete/continuous model (29), implemented in SEDPHAT version 8.01. In this model, the protein or complex of interest was treated as a single species, for which the mass and sedimentation coefficient were refined. Other species were modeled using continuous distributions. Molecular weight 1σ confidence intervals were calculated by determining a $\chi^2_{critical}$ using the F-statistic calculator in SEDPHAT, then repeating the data fitting with molecular weight fixed at a range of values, allowing other parameters to float as in the original fit. The confidence interval was determined by the extreme values that gave overall χ^2 below $\chi^2_{critical}$ (30). For the Arp2/3-VCA-actin assembly mass estimate, partial specific volume was estimated in SEDNTERP using the combined sequences of Arp2/3, two VCAs and two actin monomers. Individual materials, pairs or all three were examined in separate experiments, with example *c*(*s*) distributions (Fig. S2A) and mass measurements made for each (Fig. S2B). When present, Arp2/3 complex was present at 0.9 μM, while VCA and actin were present at 12 μM each. Individual materials showed masses consistent

with those predicted from protein sequences (except for VCA which does not sediment under these conditions).

In pairwise experiments, the sedimentation coefficients, sedimenting mass (in units of fringes) and apparent hydrodynamic masses of the mixtures showed that VCA bound Arp2/3 complex and VCA bound actin. The 9.6 S species in VCA-Arp2/3 analysis had a mass of 237 kDa, which is consistent with two VCAs bound to one Arp2/3 complex (predicted mass 241 kDa), as determined above. It should be noted however, that the lower edge of the 1σ confidence interval is also consistent with the mass of a one VCA-Arp2/3 assembly, indicating the need for a method better suited to this measurement (the multisignal method described in above). Because actin does not associate with Arp2/3 complex in absence of VCA or does so with a very weak affinity (Fig. S2B), there is no change in sedimentation coefficient or the total fringes sedimenting with Arp2/3 complex. For the mixture of actin, VCA and Arp2/3 complex, an 11.4 S complex was observed in $c(s)$ distributions for individual materials or binary mixtures. This ternary complex had an apparent mass of 333 kDa (Fig. S2B), consistent with the predicted mass for an $actin_2$:VCA_2:Arp2/3 assembly. Additionally, the "leading" peak can also be integrated in this analysis (the "lagging" peak does not completely sediment, complicating the analysis). The increase in interference signal in the 11.4 S actin-VCA-Arp2/3 complex mixture experiment at 30,000 rpm is also consistent with the $actin_2$:VCA_2:Arp2/3 assembly (giving a stoichiometry of 2.1 VCA-actins per Arp2/3 complex). In light of this overall agreement with the first method, we conclude that, when engaged with Arp2/3, both VCA peptides can accommodate an actin monomer.

Competition binding Arp2/3 affinity measurements

Competition binding experiments were performed as previously described (12), with two modifications. First, N-WASP VCA C431A C506 was labeled with Alexa Fluor 488 C5 maleimide (Invitrogen) rather than tetramethyl rhodamine. Second, a filter based plate reader was use to acquire the fluorescence polarization data (Victor 3V, Perkin Elmer), at 25˚ C. Samples were mixed and incubated (at 25˚ C) in black wall, uncoated, 384-well plates for five minutes prior to data acquisition. The polarization G-factor was inferred from the known anisotropy of the free reporter, which was used to process the remaining data into fluorescence anisotropy values. Direct binding of the reported was repeated on each day the experiment was run. Fitting of competition binding was performed using the full solution to the competition binding equilibrium found using the 'Solve' function in Mathematica 5 (Wolfram), as previously described (12).

Biotin Label Transfer

Photocrosslinking was performed on ~100 μl samples in a 1 mm path length quartz suprasil cuvette, by illuminating for 30-40 seconds with filtered (WG295, Edmund Optical) light from a 200 W Mercury Arc Lamp (Oriel). Samples were reduced using SDS-PAGE loading buffer with 5% v/v β-mercaptoethanol. Bands were resolved by SDS-PAGE and transferred to PVDF. Blots were blocked with Protein Free Blocking Agent (Pierce), probed with a 100,000-fold dilution of Neutravidin-HRP (5 mg/ml stock, Pierce). HRP was detected using chemiluminescence (Amersham ECL, GE, #RPN2209) and total protein was stained using Memcode Blue reagent (Pierce) following the manufacturer's protocol.

Supporting Information

There is an endogenous cysteine between the two V-regions of N-WASP VCA. We first used this material as a label donor and found that a low but significant amount of biotin was transferred to Arp3 and Arp2 upon illumination (Fig. S3C). This transfer to Arp3 and Arp2 was prevented by the inclusion of LatB:Actin in the reactions, and thus was due to contacts that are unlikely to occur during nucleation. Instead actin is labeled, which is unsurprising given the proximity of the actin binding sites to the label donor site. Mutating the endogenous cysteine C431 and introducing a cysteine at other sites, for example C431A, A481C (in the C-helix) allows transfer to Arp2/3 complex with higher efficiency. Deletion of the V-region from these constructs results in slightly higher overall transfer efficiency, without changing the relative intensity of transfer to Arp2/3 complex subunits (Fig. S3C). Truncation also eliminates overlap of self-labeled N-WASP species with the ArpC3, ArpC4 and ArpC5 bands (the intense bands at the bottom of Fig. S3C are due to self-labeling of VCA). Given that V-regions likely are occupied by actin during nucleation we focused on where the CA peptides of WASP proteins bound to Arp2/3 complex.

Benzoyl-phenylalanine crosslinking

N-terminally biotinylated N-WASP CA peptides with W503-BPa, where BPa is benzoyl-phenylalanine, were synthesized using FMOC methods. FMOC-BPa was obtained from Bachem. Purity was assessed by reverse phase HPLC and mass spectrometry. Crosslinking was performed as in the biotin transfer experiment, except that samples were illuminated for 18 minutes using light filtered through a 305 nm high pass glass filter (WG305, Edmund Optical). Crosslinking was assessed by SDS-PAGE

detected using Coomassie Brilliant Blue, and blotting for biotin as described above. Arp3 and ArpC1 were detected by western blot, using anti-Arp3 (sc-68395) and anti-ArpC1B (sc-48344) primary antibodies (Santa Cruz) and goat anti-mouse HRP (Biorad, #170-6516) and goat anti-rabbit HRP antibodies (Biorad, #170-6515). HRP conjugated antibodies were detected using chemiluminescence as above.

Supplemental References

1. Robinson RC, et al. (2001) Crystal structure of Arp2/3 complex. *Science* 294(5547):1679-1684.
2. Beltzner CC & Pollard TD (2004) Identification of functionally important residues of Arp2/3 complex by analysis of homology models from diverse species. *J Mol Biol* 336(2):551-565.
3. Goley ED, Rodenbusch SE, Martin AC, & Welch MD (2004) Critical conformational changes in the Arp2/3 complex are induced by nucleotide and nucleation promoting factor. *Mol Cell* 16(2):269-279.
4. Martin AC, et al. (2005) Effects of Arp2 and Arp3 nucleotide-binding pocket mutations on Arp2/3 complex function. *J Cell Biol* 168(2):315-328.
5. Rodal AA, et al. (2005) Conformational changes in the Arp2/3 complex leading to actin nucleation. *Nat Struct Mol Biol* 12(1):26-31.
6. Boczkowska M, et al. (2008) X-ray scattering study of activated Arp2/3 complex with bound actin-WCA. *Structure* 16(5):695-704.
7. Rouiller I, et al. (2008) The structural basis of actin filament branching by the Arp2/3 complex. *J Cell Biol* 180(5):887-895.

8. Zalevsky J, Grigorova I, & Mullins RD (2001) Activation of the Arp2/3 complex by the Listeria acta protein. Acta binds two actin monomers and three subunits of the Arp2/3 complex. *J Biol Chem* 276(5):3468-3475.

9. Zalevsky J, Lempert L, Kranitz H, & Mullins RD (2001) Different WASP family proteins stimulate different Arp2/3 complex-dependent actin-nucleating activities. *Curr Biol* 11(24):1903-1913.

10. Weaver AM, et al. (2002) Interaction of cortactin and N-WASp with Arp2/3 complex. *Curr Biol* 12(15):1270-1278.

11. Kreishman-Deitrick M, et al. (2005) NMR analyses of the activation of the Arp2/3 complex by neuronal Wiskott-Aldrich syndrome protein. *Biochemistry* 44(46):15247-15256.

12. Padrick SB, et al. (2008) Hierarchical regulation of WASP/WAVE proteins. *Mol Cell* 32(3):426-438.

13. Panchal SC, Kaiser DA, Torres E, Pollard TD, & Rosen MK (2003) A conserved amphipathic helix in WASP/Scar proteins is essential for activation of Arp2/3 complex. *Nat Struct Biol* 10(8):591-598.

14. Pan F, Egile C, Lipkin T, & Li R (2004) ARPC1/Arc40 mediates the interaction of the actin-related protein 2 and 3 complex with Wiskott-Aldrich syndrome protein family activators. *J Biol Chem* 279(52):54629-54636.

15. Hertzog M, et al. (2004) The beta-thymosin/WH2 domain; structural basis for the switch from inhibition to promotion of actin assembly. *Cell* 117(5):611-623.

16. Irobi E, et al. (2004) Structural basis of actin sequestration by thymosin-beta4: implications for WH2 proteins. *EMBO J* 23(18):3599-3608.

17. Chereau D, et al. (2005) Actin-bound structures of Wiskott-Aldrich syndrome protein (WASP)-homology domain 2 and the implications for filament assembly. *Proc Natl Acad Sci U S A* 102(46):16644-16649.

18. Kelly AE, Kranitz H, Dotsch V, & Mullins RD (2006) Actin binding to the central domain of WASP/Scar proteins plays a critical role in the activation of the Arp2/3 complex. *J Biol Chem* 281(15):10589-10597.

19. Leung DW, Morgan DM, & Rosen MK (2006) Biochemical properties and inhibitors of (N-)WASP. *Methods Enzymol* 406:281-296.

20. Spudich JA & Watt S (1971) The regulation of rabbit skeletal muscle contraction. I. Biochemical studies of the interaction of the tropomyosin-troponin complex with actin and the proteolytic fragments of myosin. *J Biol Chem* 246(15):4866-4871.

21. Higgs HN, Blanchoin L, & Pollard TD (1999) Influence of the C terminus of Wiskott-Aldrich syndrome protein (WASp) and the Arp2/3 complex on actin polymerization. *Biochemistry* 38(46):15212-15222.

22. Cole JL, Lary JW, T PM, & Laue TM (2008) Analytical ultracentrifugation: sedimentation velocity and sedimentation equilibrium. *Methods Cell Biol* 84:143-179.

23. Balbo A, et al. (2005) Studying multiprotein complexes by multisignal sedimentation velocity analytical ultracentrifugation. *Proceedings of the National Academy of Sciences of the United States of America* 102:81-86.

24. Padrick SB, et al. (2010) Determination of protein complex stoichiometry through multisignal sedimentation velocity experiments. *Anal Biochem* 407(1):89-103.

25. Brautigam CA, Wynn RM, Chuang JL, & Chuang DT (2009) Subunit and catalytic component stoichiometries of an in vitro reconstituted human pyruvate dehydrogenase complex. *J Biol Chem* 284(19):13086-13098.

26. Houtman JC, et al. (2006) Oligomerization of signaling complexes by the multipoint binding of GRB2 to both LAT and SOS1. *Nat Struct Mol Biol* 13(9):798-805.

27. Laue TM, Shah BD, Ridgeway RM, & Pelletier SL (1992) Computer-aided interpretation of analytical sedimentation data for proteins. *Analytical Ultracentrifugation in Biochemistry and Polymer Science*, eds Harding SE, Rowe AJ, & Horton JC (The Royal Society of Chemistry, Cambridge, UK), pp 90-125.

28. Schachman H (1992) *Analytical Ultracentrifugation in Biochemistry and Polymer Science*, eds Harding SE, Rowe AJ, & Horton JC (Royal Society of Chemistry, Cambridge), pp 3-15.

29. Boukari H, Nossal R, Sackett DL, & Schuck P (2004) Hydrodynamics of nanoscopic tubulin rings in dilute solutions. *Phys Rev Lett* 93(9):098106.

30. Bevington PR & Robinson DK (1992) *Data Reduction and Error Analysis for the Physical Sciences* (WCB McGraw-Hill) second Ed p 328.